NeuroImage 86 (2014) 164–171

Contents lists available at ScienceDirect

NeuroImage

journal homepage: www.elsevier.com/locate/ynimg

Clinical doses of atomoxetine significantly occupy both norepinephrine and serotonin transports: Implications on treatment of depression and ADHD

Y.-S. Ding [a,d,*], M. Naganawa [a], J.-D. Gallezot [a], N. Nabulsi [a], S.-F. Lin [a], J. Ropchan [a], D. Weinzimmer [a], T.J. McCarthy [b], R.E. Carson [a], Y. Huang [a], M. Laruelle [c]

[a] Department of Diagnostic Radiology, Yale University, New Haven, CT, USA
[b] Pfizer Global R&D, Groton, CT, USA
[c] New Medicines, UCB Pharma S.A., Brussels, Belgium
[d] Department of Psychiatry and Radiology, New York University, New York, NY, USA

ARTICLE INFO

Article history:
Accepted 1 August 2013
Available online 9 August 2013

Keywords:
Atomoxetine
Attention deficit hyperactivity disorder
Depression
Norepinephrine transporter
Serotonin transporter
Positron emission tomography

ABSTRACT

Background: Atomoxetine (ATX), a drug for treatment of depression and ADHD, has a high affinity for the norepinephrine transporter (NET); however, our previous study showed it had a blocking effect similar to fluoxetine on binding of [^{11}C]DASB, a selective serotonin transporter (SERT) ligand. Whether the therapeutic effects of ATX are due to inhibition of either or both transporters is not known. Here we report our comparative PET imaging studies with [^{11}C]MRB (a NET ligand) and [^{11}C]AFM (a SERT ligand) to evaluate in vivo IC_{50} values of ATX in monkeys.
Methods: Rhesus monkeys were scanned up to four times with each tracer with up to four doses of ATX. ATX or saline (placebo) infusion began 2 h before each PET scan, lasting until the end of the 2-h scan. The final infusion rates were 0.01–0.12 mg/kg/h and 0.045–1.054 mg/kg/h for the NET and SERT studies, respectively. ATX plasma levels and metabolite-corrected arterial input functions were measured. Distribution volumes (V_T) and IC_{50} values were estimated.
Results: ATX displayed dose-dependent occupancy on both NET and SERT, with a higher occupancy on NET: IC_{50} of 31 ± 10 and 99 ± 21 ng/mL plasma for NET and SERT, respectively. At a clinically relevant dose (1.0–1.8 mg/kg, approx. 300–600 ng/mL plasma), ATX would occupy >90% of NET and >85% of SERT. This extrapolation assumes comparable free fraction of ATX in humans and non-human primates.
Conclusion: Our data suggests that ATX at clinically relevant doses greatly occupies both NET and SERT. Thus, therapeutic modes of ATX action for treatment of depression and ADHD may be more complex than selective blockade of NET.

Introduction

Atomoxetine (ATX, Strattera) is the first non-stimulant drug that was approved for the treatment of attention-deficit/hyperactivity disorder (ADHD) (Arnsten, 2006; Bymaster et al., 2002; Chamberlain et al., 2007a; Del Campo et al., 2011; Michelson et al., 2001; Swanson et al., 2006; Volkow et al., 2001). It has also been used to improve responses to treatment of depression (Dell'Osso et al., 2010; O'Sullivan et al., 2009). The majority of medications currently used in the treatment of ADHD or depression act to increase brain catecholamine levels; e.g., dopamine (DA), norepinephrine (NE) and serotonin. However, the precise mechanisms that are responsible for the therapeutic effects of these medications remain elusive. For example, based on the current literature, the therapeutic effects of methylphenidate, the most common treatment for ADHD, are due mostly to its dopamine transporter (DAT) inhibition. However, our recent in vivo PET imaging study demonstrated, for the first time in humans, that oral methylphenidate significantly occupies norepinephrine transporter (NET) at clinically relevant doses with an ED_{50} of 0.14 mg/kg, which is lower than that for DAT (0.25 mg/kg), suggesting the potential relevance of NET inhibition in the therapeutic effects of methylphenidate in ADHD (Hannestad et al., 2010).

ATX is another effective drug for the treatment of ADHD, belonging to a different structural class than methylphenidate (being a distant relative of tricyclics). It is thought that ATX acts via blockade of the presynaptic norepinephrine transporter (NET) in the brain; however, our previous study showed that it had a blocking effect similar to fluoxetine (a selective serotonin transporter [SERT] inhibitor) on binding of [^{11}C]DASB (Ding and Fowler, 2005), a selective SERT ligand with a Ki value of 1.77 nM (Houle et al., 2000). These results suggested that ATX not only binds to NET, but also binds to SERT with high affinity. To date, whether the therapeutic effects of ATX in the treatment of either ADHD or depression are due to inhibitory effects on one (NET) or two transporters (NET

* Corresponding author at: New York University School of Medicine, 660 First Avenue, 4th Floor, New York, NY 10016, USA. Fax: +1 212 263 7541.
E-mail addresses: yu-shin.ding@nyumc.org, yushin.ding@nyu.edu (Y.-S. Ding).

1053-8119/$ – see front matter © 2013 Published by Elsevier Inc.
http://dx.doi.org/10.1016/j.neuroimage.2013.08.001

and SERT) is not known. The aim of this investigation was to carry out comparative occupancy studies with [^{11}C]MRB (a NET ligand) (Ding et al., 2003, 2005, 2006); and [^{11}C]AFM ([^{11}C]2-[2-(dimethylaminomethylphenylthio)]-5-fluoromethylphenylamine, a SERT ligand with a Ki value of 0.42 nM) (Huang et al., 2002) to evaluate the in vivo IC_{50} of ATX for both NET and SERT in non-human primates (NHP) using positron emission tomography (PET) imaging.

In order to maintain a constant concentration of ATX in the plasma during the PET acquisition time, a continuous infusion protocol was used for both occupancy studies. The detailed evaluation and discussion on the suitability of [^{11}C]MRB for drug occupancy studies of NET with ATX has been published (Gallezot et al., 2011). We report here the detailed evaluation of the SERT occupancy study with ATX using [^{11}C]AFM. A direct comparison of the outcome of these two studies and their potential implication on the therapeutic mechanisms of ATX will also be discussed.

Materials and methods

Study design

The continuous infusion protocol was similar to our previous study with [^{11}C]MRB (Gallezot et al., 2011). Two infusion rates were used: 2 h before the beginning of each post-ATX PET scan, the first ATX infusion at the "loading" rate was begun; then, 1 h before the injection of [^{11}C]AFM and the beginning of the PET scan, the infusion rate was lowered by 37.5% (i.e., "maintenance" rate). This infusion rate was maintained until the end of PET scan. Two monkeys were scanned with maintenance rates: 0.045 mg/kg/h (low dose), 0.135 mg/kg/h (medium dose), and 0.405 mg/kg/h (high dose). One monkey was scanned with the higher maintenance rates: 0.135 mg/kg/h (medium dose), 0.405 mg/kg/h (high dose), and 1.054 mg/kg/h (very high dose). The design was to have each monkey to be scanned for a total of four times on two study days. These two study days were scheduled at least three weeks apart to allow recovery from the effect of the anesthesia and blood drawing. On each study day, two PET scans were acquired, beginning 4 h apart. The first study day consisted of the baseline and medium-dose scans, the second study day consisted of the low- and high-dose scans.

Study population

The study protocol was approved by the Yale University Institutional Animal Care and Use Committee. Three monkeys were scanned. One monkey was scanned four times at the higher maintenance rates. Due to the unavailability of arterial blood sampling, the other monkeys were scanned twice (baseline and low-dose for one, baseline and medium-dose for another). The monkeys ranged in age from four to eight years old and body weight from 6.2 to 9.1 kg.

Radiochemistry

[^{11}C]AFM was prepared by *N*-methylation of the precursor with [^{11}C]methyl triflate using the PETtrace cyclotron, MeI Microlab®, and TRACERLab™ FXC automated synthesizer (GE Healthcare, Chalfont St Giles, UK). Briefly, [^{11}C]methyl triflate was trapped in 400 μL anhydrous methyl ethyl ketone containing 0.5–1 mg precursor at 0 °C, and the resulting mixture was heated for 1 min at 60 °C, and then purified by RP-HPLC. The PET drug was isolated by solid phase extraction and formulated into 9% ethanolic saline, then passed through a 0.22 μm membrane filter for final sterilization. The average chemical and radiochemical purities were >99.9% and 93.5 ± 3.5% (n = 8). The average injected dose was 250 ± 17 MBq with average injected mass of 0.81 ± 0.45 μg.

PET imaging

Animals were initially anesthetized with a ketamine hydrochloride (10 mg/kg, IM), and then transported to the PET suite for scan preparation at least 2 h prior to the initial PET scan. Once intubated, the animals were maintained on oxygen and isoflurane (~1.5%) anesthesia. Scans were performed with the High Resolution Research Tomograph (HRRT) (Siemens/CTI, Knoxville, TN, USA) PET scanner which acquires 207 simultaneous slices with 1.2 mm inter-slice distance and resolution of ~3 mm. Following a 6-min transmission scan, [^{11}C]AFM was injected over 2 min by an infusion pump (Harvard PHD 22/2000, Harvard Apparatus, Holliston, Massachusetts, USA). List-mode data were acquired for 120 min. Dynamic scan data were reconstructed with all corrections (attenuation, normalization, scatter, randoms, and deadtime) using the MOLAR algorithm (Carson et al., 2003; Johnson et al., 2004). A sequence of 33 frames was reconstructed with the following timing: 6 × 30 s, 3 × 1 min, 2 × 2 min, and 22 × 5 min.

Arterial input function measurement

In order to measure the time–concentration curve of [^{11}C]AFM, 21 blood samples were drawn at 0.5, 1, 1.5, 2, 2.5, 3, 4, 6, 8, 10, 15, 20, 25, 30, 40, 50, 60, 75, 90, 105, and 120 min after the injection of [^{11}C]AFM. Sample volumes were approximately 0.5 mL. Samples drawn at 3, 6, 15, 30, 60, and 90 min postinjection had a volume of 1.5 mL in order to measure the fraction of unchanged [^{11}C]AFM in plasma by HPLC. Plasma was separated from blood cells by centrifugation (3900 *g* for 5 min at 4 °C; Allegra X-22R Centrifuge, Beckman Coulter, Fullerton, CA, USA). Whole blood and plasma samples were counted in a cross-calibrated well counter (Wizard 1480, Perkin Elmer, Waltham, MA, USA). Plasma proteins were precipitated using equal amounts of acetonitrile and centrifugation at 14,000 *g* for 5 min. The supernatant was counted and 0.2 mL was analyzed by reverse-phase HPLC with a Luna C18(2) column (semi-prep, 10 × 250 mm, 10 μm, Phenomenex, Torrance, CA, USA). The column was eluted with a mixture of acetonitrile and aqueous 0.1 M ammonium formate pH 4.2 (32/68) at a flow rate of 4.3 mL/min. The parent fraction was calculated as the ratio of the total radioactivity in fractions containing the parent compound to the total radioactivity collected, and fitted to a sum of exponentials (f_H). In addition, the time-varying extraction efficiency of radioactivity in acetonitrile was measured from the counts in the supernatant and the pellet. The extraction fractions were fitted to a polynomial curve (f_S). The final unchanged tracer fraction in plasma was then computed as the product of the functions f_S and f_H.

[^{11}C]AFM plasma free fraction

The procedure for measurement of plasma free fraction (f_p) of [^{11}C]AFM was identical to that used in our previous study with [^{11}C]MRB (Gallezot et al., 2011). Briefly, for measurement of tracer plasma free fraction (f_p), ~740 kBq of [^{11}C]AFM was added (~25 μl/mL blood from the dose vial) to a blood sample withdrawn before injection to produce a blood standard. After mixing and centrifugation of red blood cells, plasma filtrate was separated from plasma proteins using ultrafiltration tubes (Centrifree UF device number 4104, Millipore, Billerica, MA, USA) and centrifugation (1100 *g* for 20 min; EC Medilite Centrifuge, Thermo Fisher Scientific, Waltham, MA, USA). Plasma and filtrate samples were counted in triplicate and free fraction (f_p) was estimated as the ratio of the mean concentrations in filtrate and plasma.

ATX plasma levels

In addition to the samples used to determine [^{11}C]AFM radioactivity concentration in plasma, four 3-mL blood samples were drawn 60, 120, 180, and 240 min post-ATX infusion to determine the ATX concentration in plasma. The plasma level of ATX was quantified with capillary

gas chromatography–mass spectrometry (Analytical Psychopharmacology Laboratory, Nathan Kline Institute, NY, USA).

Magnetic resonance imaging and regions of interest

T1-weighted MR images were acquired for each rhesus monkey on a Siemens 3 T Trio scanner and co-registered with PET images. In order to compute regional time activity curves, selected regions of interest (ROIs) where drawn on a template brain (a representative MR image of a monkey brain) for the brainstem (1.85 cm^3), thalamus (0.25 cm^3), globus pallidus (0.12 cm^3), insula (0.96 cm^3), putamen (0.38 cm^3), caudate nucleus (0.43 cm^3), hippocampus (0.32 cm^3), amygdala (0.097 cm^3), temporal lobe (3.18 cm^3), anterior cingulate cortex (0.077 cm^3), cingulate cortex (0.64 cm^3), occipital lobe (5.22 cm^3), frontal lobe (2.49 cm^3), and cerebellum white matter (0.51 cm^3), and cerebellum (5.91 cm^3). To transfer the template of regions to the MR image of each monkey, an affine 12-parameter coregistration matrix was estimated using a normalized mutual information algorithm (FLIRT).

Estimation of [^{11}C]AFM volume of distribution and ATX IC_{50} and ED_{50}

Although the cerebellum is accepted as reference region for SERT studies, existence of some specific binding in the cerebellum has been reported (Hinz et al., 2008; Kish et al., 2005; Parsey et al., 2006; Szabo et al., 2002). Given the higher affinity of AFM than DASB, we chose not to compute binding potential. Instead, we used the occupancy plot, which was originally introduced by Lassen et al. (1995), and subsequently by Cunningham et al. (2010). The occupancy plot uses regional estimates of volume of distribution (V_T), and can be used in the absence of a reference region. Regional V_T values of [^{11}C]AFM were estimated using the multilinear analysis method (MA1) (Ichise et al., 2002). When MA1 was applied to the regional time activity curves, t^* was set to 40 min after administration. Standard errors of V_T and V_T/f_p were estimated using the error propagation equation. Using the volume of distribution corrected for the plasma free fractions (V_T/f_p) transporter occupancy (Occ) was calculated as the slope of the occupancy plot from the following equation:

$$\frac{V_T}{f_p}(\text{post-drug}) - \frac{V_T}{f_p}(\text{baseline}) = Occ\left(\frac{V_T}{f_p}(\text{baseline}) - \frac{V_{ND}}{f_p}\right).$$

Then, ATX IC_{50} was estimated by fitting the ATX occupancy values obtained from multiple experiments versus the ATX plasma concentration (C_{ATX}) using the following equation:

$$Occ = \frac{C_{ATX}}{C_{ATX} + IC_{50}}$$

The IC_{50} estimates [ng/mL plasma] were converted to ED_{50} estimates [mg/kg/h] using the linear correlation between the measured ATX plasma levels and the infusion rates.

Results

ATX plasma levels

For all monkey studies, ATX plasma levels could be considered stable 120 min after the beginning of the first infusion for all doses (low, medium, high and very high doses), ranging between 50 ng/mL and 1132 ng/mL (Fig. 1A). Moreover, average ATX plasma levels and the infusion rate were well correlated (Fig. 1B). The slope of the regression line was 1.12 kg × h/L ($r^2 = 0.96$, $n = 5$, intercept was set to zero).

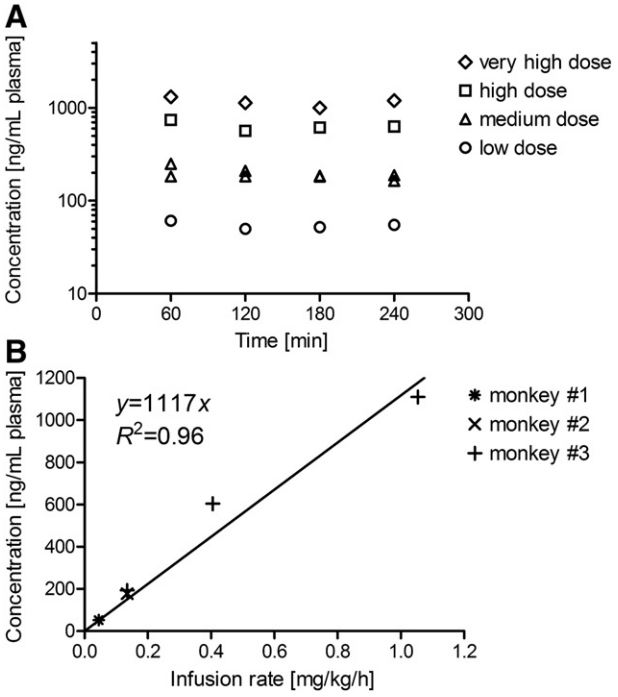

Fig. 1. (A) ATX plasma concentration measured for monkeys, for the low (circle), medium (triangle), high (square), and very high (diamond) dose scans (total 5 scans) plotted on semilog scale. (B) Correlation between the ATX plasma levels (average of time points 120, 180, and 240 min) and the maintenance infusion rates for monkey #1 (*), #2 (×) and #3 (+), respectively. The regression line was obtained from ATX plasma concentrations averaged over 3 time points (120, 180, and 240 min) and infusion rate (slope = 1.12 kg × h/L, $r^2 = 0.960$, $n = 5$).

[^{11}C]AFM input function

The fraction of unmetabolized [^{11}C]AFM in plasma decreased rapidly (Fig. 2A) with parent fractions of 38 ± 5% and 8 ± 5% at 6 and 30 min post-injection, respectively. [^{11}C]AFM plasma free fraction was reasonably stable from scan to scan (Fig. 2B) (22% ± 4%, $n = 8$) and larger than that reported previously in baboons (9.6 ± 0.5%, $n = 4$, Huang et al., 2002).

[^{11}C]AFM distribution volumes

Fig. 3 shows typical regional time-activity curves and fits to the MA1 model for a baseline scan with t^* set to 40 min. The distribution volume (V_T) values of [^{11}C]AFM are shown in Table 1. In baseline scans, regional brain [^{11}C]AFM distribution volume reflected the known distribution of SERT, with high binding in the brainstem and thalamus, intermediate binding in neocortex, and lowest binding in the cerebellum. Parametric images of V_T from monkey #3 are shown in Fig. 4, providing visualization of dose-dependent occupancy. V_T values were reduced throughout the brain at all doses (Fig. 5). In particular, V_T in the cerebellum was reduced by 48% (monkey #1), 29% (monkey #2), and 22 ± 8% (monkey #3), suggesting that there was some contribution of specific binding to the cerebellum signal.

Estimating ATX IC_{50} using occupancy plot

Occupancy plots with the normalized distribution volumes are shown in Figs. 5A–C. ATX occupancy was estimated for each scan as the slope of the regression line. The ATX occupancy estimates were 46% for the low dose scan for monkey #1 (Fig. 6A), 58% for the medium dose scan for monkey #2 (Fig. 6B), and 64%, 79%, and 92% for the medium-, high-, and very high-dose scans for monkey #3 (Fig. 6C). The relationship between the ATX occupancy estimates and the measured concentration

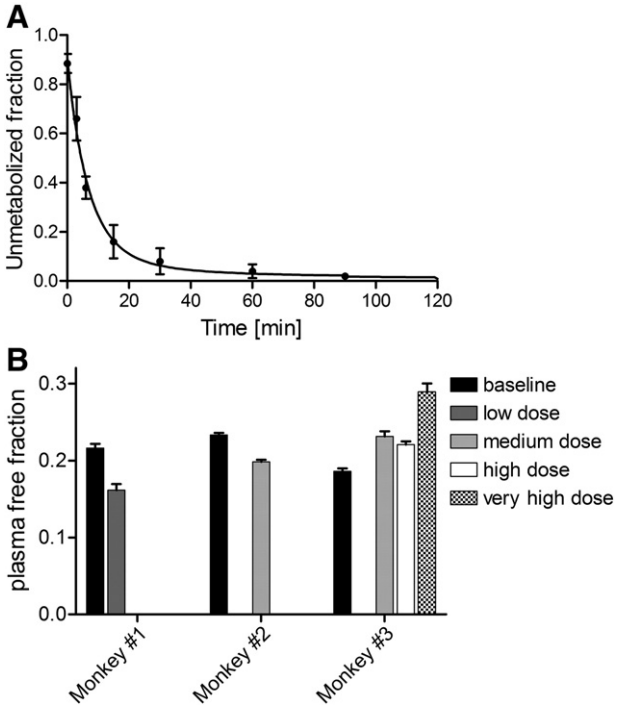

Fig. 2. (A) Unchanged fraction of [^{11}C]AFM in plasma (mean ± SD, $n = 8$). The solid line represents the average of the fitted parent fraction curves used for metabolite correction. (B) [^{11}C]AFM plasma free fraction measured by ultrafiltration for the baseline (black), low (dark gray), medium (medium gray), high (white), and very high (checker pattern) ATX dose scans. Error bars represent the standard errors estimated from the triplicate measurements of plasma and ultrafiltrate samples.

of ATX in plasma is shown in Fig. 6D. The ATX IC_{50} computed with the normalized distribution volume was estimated to be 99 ng/mL (relative standard error (rSE) = 21%) of plasma ATX concentration, which corresponds to an infusion rate of 0.088 mg/kg/h. If the calculation was performed without normalization by f_p, the ATX IC_{50} estimate was very similar, 87 ng/mL, but with higher uncertainty (rSE = 41%).

Summary of the comparative occupancy studies of ATX for NET (using [^{11}C]MRB) and SERT (using [^{11}C]AFM)

ATX displayed dose-dependent occupancy of both NET and SERT, with a higher occupancy of NET: IC_{50} of 31 ± 10 and 99 ± 21 ng/mL

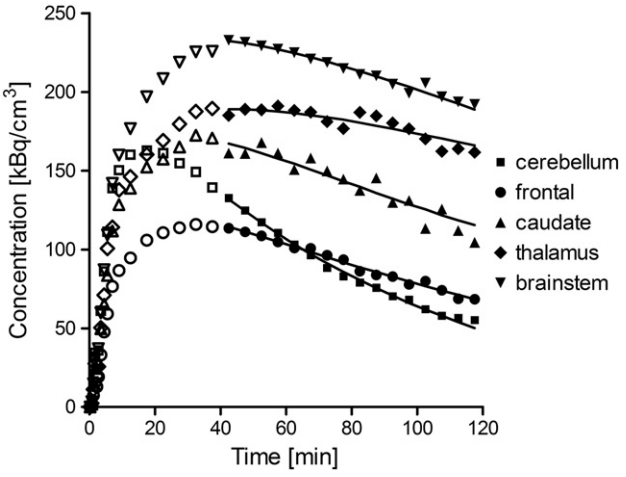

Fig. 3. Regional time-activity curves in one monkey (#3) at baseline scan. Typical examples of MA1 fitting are shown ($t^* = 40$ min). ROIs are cerebellum (squares), frontal lobe (circles), caudate (triangles), thalamus (diamonds), and brainstem (downward-triangles). Points used for the estimation are shown as closed symbols.

Table 1
[^{11}C]AFM distribution volumes (V_T).

Region	Monkey	Distribution volume V_T [mL/cm^3]				
		Baseline	ATX low dose	ATX medium dose	ATX high dose	ATX very high dose
Cerebellum	#1	42.1	21.9			
	#2	37.2		26.2		
	#3	36.3		31.0	28.2	25.3
Frontal lobe	#1	47.2	24.2			
	#2	45.2		32.0		
	#3	42.1		32.0	29.3	27.8
Caudate	#1	101.0	53.8			
	#2	76.3		45.5		
	#3	74.2		49.9	40.2	31.4
Thalamus	#1	118.9	53.1			
	#2	111.8		59.3		
	#3	142.3		67.1	52.1	37.7
Brainstem	#1	162.4	67.4			
	#2	129.4		59.4		
	#3	141.1		86.5	56.9	41.8

plasma for NET and SERT, respectively (Gallezot et al., 2011). At a clinically relevant dose (1.0–1.8 mg/kg, approx. 300–600 ng/mL plasma), ATX would occupy >90% of NET and >85% of SERT. This extrapolation assumes comparable free fraction of ATX in humans and NHP.

Discussion

Occupancy analysis

In our previous study, variability in the V_T estimates was observed using [^{11}C]MRB post-ATX (Gallezot et al., 2011). A dose-dependent reduction was found when the V_T was normalized with free fraction (V_T/f_p). Normalization of V_T with f_p should, in principle, reduce variability in V_T if variability in f_p is substantial and if it is measured accurately. In this study using [^{11}C]AFM with ATX, we could see a dose-dependent reduction using either V_T or V_T/f_p. However, the fitting of the occupancy curve (Fig. 6D) and the precision of the ATX IC_{50} estimate were improved using the normalized distribution volume. Therefore, V_T/f_p was used as the primary outcome parameter in this study as well.

Selectivity of ATX

Earlier literature indicated that ATX is an equally potent inhibitor of both NET and SERT. Based on the in vitro data previously shown, (R)-[^{3}H]tomoxetine (a.k.a. atomoxetine) bound not only to the NET but also to the SERT with an affinity (Kd) of 8.9 and 2 nM for human SERT and NET, respectively (Tatsumi et al., 1997). These results were consistent with our previous study that showed that ATX had a blocking effect similar to fluoxetine (a selective serotonin transporter [SERT] inhibitor) on binding of [^{11}C]DASB (Ding and Fowler 2005). Our comparative occupancy studies with [^{11}C]MRB (Gallezot et al., 2011) and [^{11}C]AFM (current study) to evaluate the in vivo IC_{50} of ATX for both NET and SERT using PET in NHP further corroborate the selectivity of ATX.

Comparison of binding affinity estimates in vivo versus in vitro

Based on our studies, ATX displayed IC_{50} of 31 ± 10 and 99 ± 21 ng/mL plasma for NET and SERT, respectively. It is worth noting that this value of 3.2 for the selectivity ratio of ATX towards NET vs. SERT measured via in vivo PET imaging in NHP is close in magnitude to the selectivity ratio of 4.5 derived from the previously reported in vitro Kd values using human NET and SERT tissue homogenates (Tatsumi et al., 1997).

It is known that ATX is metabolized through the cytochrome P-450 2D6 (CYP2D6) enzyme system (Ring et al. 2002). Approx. 7% of patients

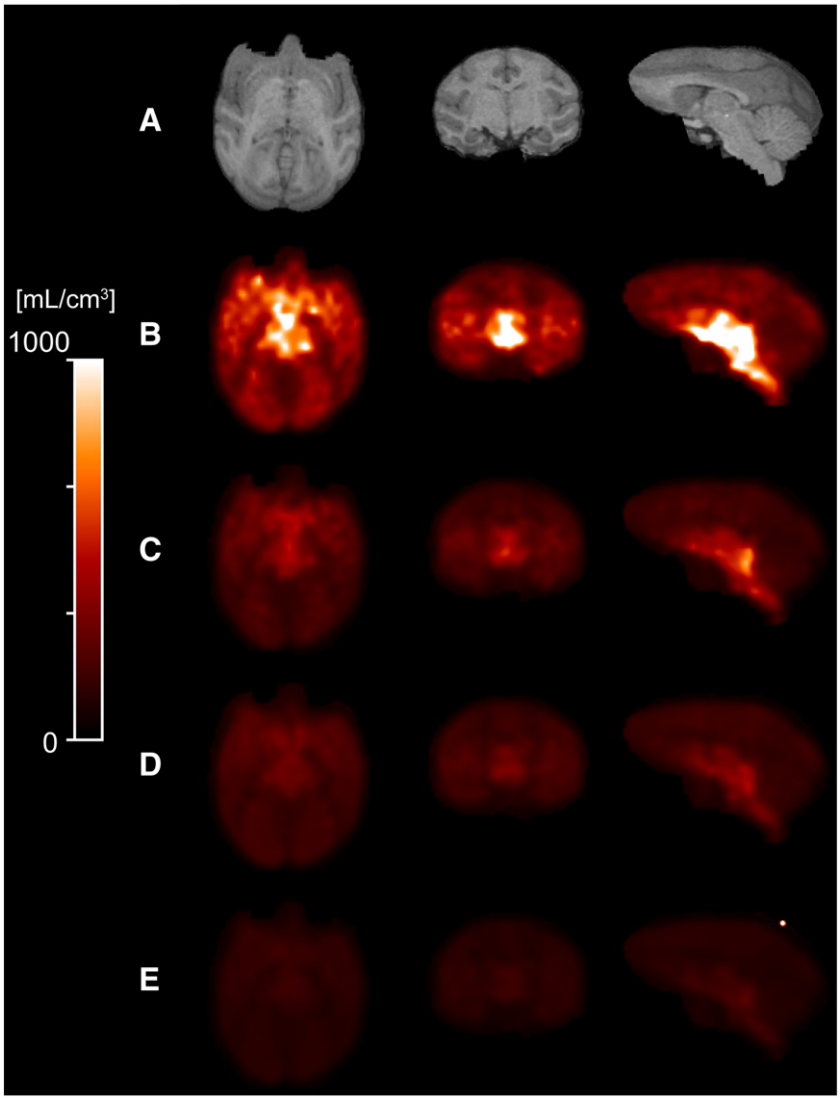

Fig. 4. A) Coregistered MR anatomic images. Parametric images of normalized distribution volume for monkey#3 at B) baseline and after blockade with C) 0.135 mg/kg/h, D) 0.405 mg/kg/h, and E) 1.054 mg/kg/h of ATX.

are CYP2D6 poor metabolizers (PM); i.e., most are extensive metabolizers (EM). The primary oxidative metabolite of atomoxetine is 4-hydroxyatomoxetine, which is subsequently conjugated to form the corresponding glucuronidate. Although differences were observed in the excretion and relative amounts of metabolites formed, the primary difference observed between EM (extensive metabolizer) and PM (poor metabolizer) subjects was the rate at which atomoxetine was biotransformed to 4-hydroxyatomoxetine. Within 24 h postdose of [^{14}C]-atomoxetine, ~90% of the total radioactive dose had been excreted by EM subjects, whereas only 27% of the total dose was excreted by PM subjects (Sauer et al., 2003). It has also been shown that atomoxetine was highly bound to plasma protein. The plasma protein binding of total radioactivity at 2 h after administration of [^{14}C]-atomoxetine in EM subjects and PM subjects was 54% and 97%, respectively, suggesting that the net free fraction of total C-14 in plasma (a combination of ATX and metabolites) varies with metabolism, and ATX has much higher protein binding than metabolites. The metabolic profile, the extent of metabolism rate and the free fraction of ATX in NHP have not been well characterized. Thus, it is difficult to relate the in vivo ATX IC_{50} plasma concentration in NHP (31 ng/mL, 106 nM for NET; or 99 ng/mL, 339 nM for SERT) with the previously reported Kd values for human in vitro (2 nM and 8.9 nM for NET and SERT, respectively). Furthermore, the difference between in vivo and in vitro Kd might be due to error in free fraction in plasma (but also are potentially sensitive to free fractions of the two PET tracers in brain), gradient across the blood–brain barrier or assay conditions, etc. Interestingly, if NHP are poor metabolizers with the 3% free fraction, the in vivo IC_{50} measurement would be a perfect match with the in vitro affinity (i.e., 3 nM = 106 × 0.03 for NET affinity; or 9 nM = 339 nM × 0.03 for SERT affinity).

Noradrenergic action in ADHD and depression

ADHD is a major psychiatric disorder in children, but effective treatments remain elusive and the neurochemical mechanisms of this disorder are poorly understood. It has been widely accepted that the cognitive and behavioral impairment characteristics of ADHD are caused by the dysregulation in dopamine (DA) and norepinephrine (NE) circuits (American Psychiatric Press, 1994; Barkley, 1997; Dopheide and Pliszka, 2009). The role of NE in ADHD is supported by animal studies showing that many of the symptoms of ADHD can be recreated by blocking α-2 NE receptors in the prefrontal cortex (PFC) (Arnsten, 2009; Chappell et al., 1995; Horrigan and Barnhill, 1995; Hunt et al., 1995; Ma et al.,

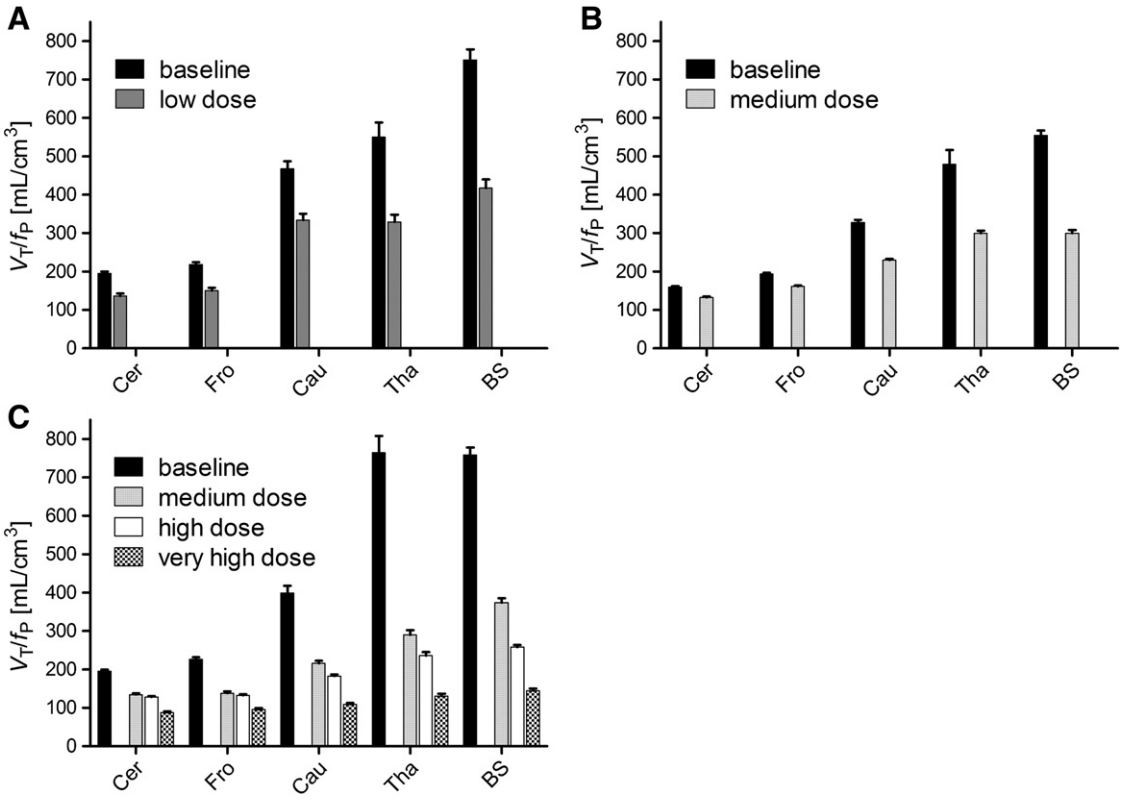

Fig. 5. Dose-dependent occupancy of ATX in three monkeys. (A to C) Normalized distribution volumes (V_T/f_p) using MA1 at baseline (black), the low (dark gray), medium (medium gray), high (light gray), and very high (white) doses are shown for the brain regions (Cer = cerebellum, Fro = frontal lobe, Cau = caudate, Tha = thalamus, BS = brainstem) in each monkey. Error bars represent the estimated standard errors.

2003; Scahill et al., 2001). The most compelling evidence supporting the role of DA and NE in ADHD comes from treatment studies. Medications used in the treatment of ADHD (including methylphenidate, dextroamphetamine and atomoxetine) act to increase brain DA and NE. For example, the most widely prescribed pharmacological treatment for patients with ADHD has been methylphenidate (MP, Ritalin). Though most studies have focused on its effects on the dopamine system, we have recently demonstrated that oral MP significantly occupies NET at clinically relevant doses with an ED_{50} of 0.14 mg/kg for NET, lower than that for DAT (0.25 mg/kg), suggesting the role of NET inhibition in the therapeutic effects of drugs for treatment of ADHD (Hannestad et al., 2010).

The noradrenergic action also exerts an important clinical effect in different antidepressant classes such as desipramine and nortriptyline (tricyclics, prevalent noradrenergic effect), reboxetine and atomoxetine (relatively pure noradrenergic reuptake inhibitor (NRIs)), and dual action antidepressants such as the serotonin noradrenaline reuptake inhibitors (SNRIs), the noradrenergic and dopaminergic reuptake inhibitor (NDRI) bupropion, and other compounds (e.g., mianserin, mirtazapine), which enhance the noradrenergic transmission. Even some atypical antipsychotics, such as quetiapine, and its metabolite norquetiapine in particular, act on the noradrenergic system binding the NET.

The development of ATX and its approval for the treatment of ADHD by the Food and Drug Administration (Faraone et al., 2005) were based on the rationale that it selectively blocks the NET (Barton, 2005) and increases the availability of intrasynaptic NE, resulting in the improvement of high-level cognitive functions that are often impaired in ADHD, such as working memory and inhibitory response control (Robbins and Arnsten, 2009). In principle, ATX may offer clinical advantages by virtue of its limited effects on subcortical dopamine, which is thought to be responsible for the abuse potential of psychostimulant treatment (Volkow et al., 2001). Furthermore, this single NE pathway of drug mechanism may facilitate further drug research and development. However, based on our current in vivo PET imaging studies, ATX at clinically relevant doses greatly occupies both NET and SERT. Thus, the interpretation of its therapeutic effect for treatment of depression and ADHD is more complex than the current thinking.

The mechanism actions of ATX in ADHD and depression

It has been shown that response inhibition (the ability to exert high-level inhibitory control over motor responses so as to suppress unwanted actions) is impaired in subjects with ADHD and is one of the most robust cognitive findings in ADHD research (Lijffijt et al., 2005). The deficits of inhibition control (a.k.a. impulsivity) can be measured by the stop-signal task (SST), and quantified by the stop-signal reaction time (SSRT), an estimate of the time taken to inhibit the prepotent motor response (Aron et al., 2003). The research group at Cambridge, UK found that single doses of atomoxetine (60 mg) were able to improve response inhibition in humans and in rats (Bari et al., 2009; Chamberlain et al., 2006, 2007a; Eagle et al., 2008). By contrast, serotonin manipulations with citalopram, a SERT blocker (Chamberlain et al., 2006, Del Campo et al., 2011), or with Buspirone, a serotonin 5-HT1A receptor (Chamberlain et al., 2007b) appear to have no behavioral effects on the SSRT. These results suggest that atomoxetine enhances stopping selectively via actions on NE uptake, and that NET drugs may be more suited to ameliorating impaired response inhibition as an ADHD therapeutic target.

Taken together, the inhibitory effect of ATX on NET plays a crucial role on its therapeutic effect on ADHD, while the inhibitory effect of ATX on SERT may play a more important role on its therapeutic effect on depression. Further studies to elucidate the actual relationship between the drug mechanisms and drug therapeutic effects are needed.

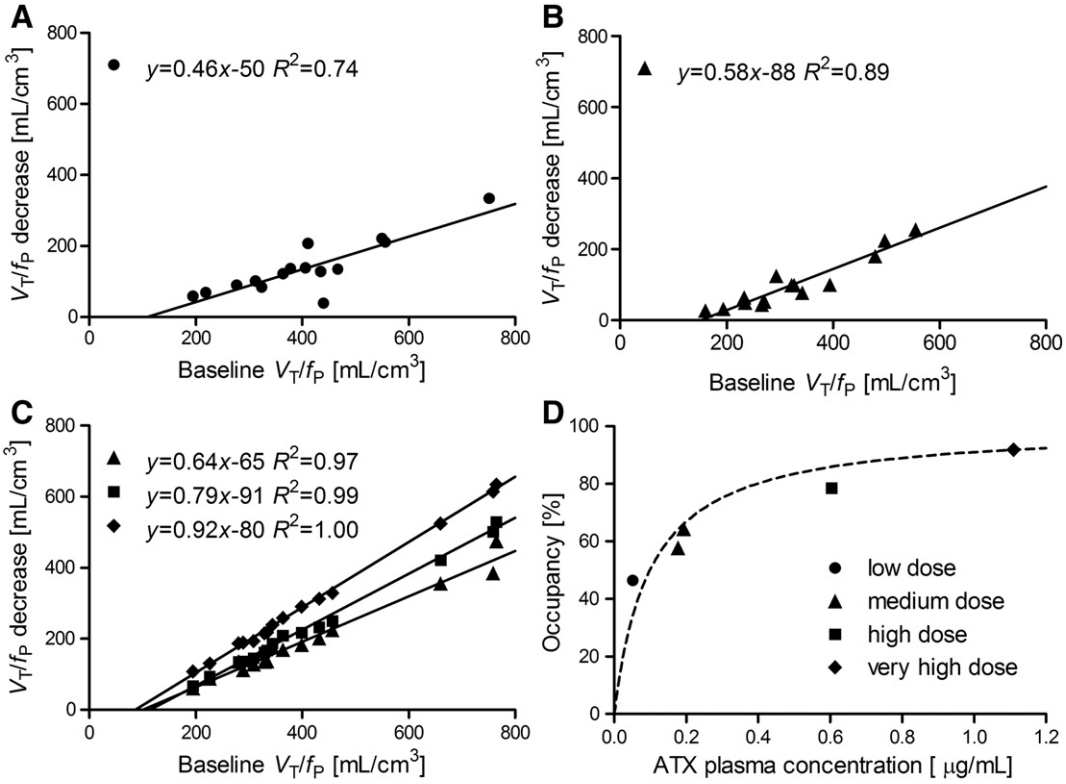

Fig. 6. Occupancy plots (A to C) for monkeys #1, #2 and #3 are displayed as regression lines: low dose (circles), medium dose (triangles), high (squares) and very high doses (diamonds). (D) The occupancy curve was fitted using the estimated occupancies and the ATX plasma concentration. IC_{50} was estimated at 99 [ng/mL].

Acknowledgment

The authors thank the staff of the Yale University PET Center for their technical expertise and support, and Tom Cooper at Nathan S. Kline Institute for Psychiatric Research (Orangeburg, New York) for measuring blood levels of atomoxetine for this study. Funding for the ATX-NET study and the ATX-SERT study was provided by the Yale Pfizer and Yale GSK Bioimaging Alliance, respectively.

Conflict of interest

Marc Laruelle is a full-time employee of UCB Pharma, and a GSK shareholder. Timothy McCarthy is a full time employee of Pfizer, Inc. None of the other authors reports any biomedical financial interests or potential conflicts of interests.

References

American Psychiatric Press, 1994. Diagnostic and Statistical Manual of Mental Disorders, Fourth Edition, Fourth edition. American Psychiatric Association, Washington, DC.

Arnsten, A.F., 2006. Fundamentals of attention-deficit/hyperactivity disorder: circuits and pathways. J. Clin. Psychiatry 67 (Suppl. 8), 7–12.

Arnsten, A.F., 2009. Toward a new understanding of attention-deficit hyperactivity disorder pathophysiology: an important role for prefrontal cortex dysfunction. CNS Drugs 23 (Suppl. 1), 33–41.

Aron, A.R., Fletcher, P.C., Bullmore, E.T., Sahakian, B.J., Robbins, T.W., 2003. Stop-signal inhibition disrupted by damage to right inferior frontal gyrus in humans. Nat. Neurosci. 6, 115–116.

Bari, A., Eagle, D.M., Mar, A.C., Robinson, E.S., Robbins, T.W., 2009. Dissociable effects of noradrenaline, dopamine, and serotonin uptake blockade on stop task performance in rats. Psychopharmacology (Berl) 205, 273–283.

Barkley, R.A., 1997. Attention Deficit Hyperactivity Disorder: A Handbook for Diagnosis and Treatment. The Guilford Press, New York.

Barton, J., 2005. Atomoxetine: a new pharmacotherapeutic approach in the management of attention deficit/hyperactivity disorder. Arch. Dis. Child. 90 (Suppl. 1), i26–i29.

Bymaster, F.P., Katner, J.S., Nelson, D.L., Hemrick-Luecke, S.K., Threlkeld, P.G., Heiligenstein, J.H., Morin, S.M., et al., 2002. Atomoxetine increases extracellular levels of norepinephrine and dopamine in prefrontal cortex of rat: a potential mechanism for efficacy in attention deficit/hyperactivity disorder. Neuropsychopharmacology 27, 699–711.

Carson, R.E., Barker, W.C., Liow, J.S., Adler, S., Johnson, C.A., 2003. Design of a motion-compensation OSEM list-mode algorithm for resolution–recovery reconstruction of the HRRT. Conference Record of the IEEE Nuclear Science Symposium and Medical Imaging Conference M16-6. Nuclear Science Symposium Conference Record, IEEE, 5, pp. 3281–3285 (http://ieeexplore.ieee.org/xpls/abs_all.jsp?arnumber_1352597).

Chamberlain, S.R., Müller, U., Blackwell, A.D., Clark, L., Robbins, T.W., Sahakian, B.J., 2006. Neurochemical modulation of response inhibition and probabilistic learning in humans. Science 311 (5762), 861–863.

Chamberlain, S.R., Müller, U., Deakin, J.B., Corlett, P.R., Dowson, J., Cardinal, R.N., Aitken, M.R., Robbins, T.W., Sahakian, B.J., 2007a. Lack of deleterious effects of buspirone on cognition in healthy male volunteers. J. Psychopharmacol. 21, 210–215.

Chamberlain, S.R., Del Campo, N., Dowson, J., Müller, U., Clark, L., Robbins, T.W., Sahakian, B.J., 2007b. Atomoxetine improved response inhibition in adults with attention deficit/hyperactivity disorder. Biol. Psychiatry 62, 977–984.

Chappell, P.B., Riddle, M.A., Scahill, L., et al., 1995. Guanfacine treatment of comorbid attention deficit hyperactivity disorder and Tourette's syndrome: preliminary clinical experience. J. Am. Acad. Child Adolesc. Psychiatry 34, 1140–1146.

Cunningham, V.J., Rabiner, E.A., Slifstein, M., Laruelle, M., Gunn, R.N., 2010. Measuring drug occupancy in the absence of a reference region: the Lassen plot re-visited. J. Cereb. Blood Flow Metab. 30, 46–50.

Del Campo, N., Chamberlain, S.R., Sahakian, B.J., Robbins, T.W., 2011. The roles of dopamine and noradrenaline in the pathophysiology and treatment of attention-deficit/hyperactivity disorder. Biol. Psychiatry 69, e145–e157.

Dell'Osso, B., Palazzo, M.C., Oldani, L., Altamura, A.C., 2010. The noradrenergic action in antidepressant treatments: pharmacological and clinical aspects. CNS Neurosci. Ther. 17, 23–32.

Ding, Y.-S., Fowler, J.S., 2005. New generation radiotracers for nAChR and NET. Proceedings of the third La Jolla Conference "The Magic Bullet a Century Later". Nucl. Med. Biol., 32, pp. 707–718 (Review).

Ding, Y.-S., Lin, K.S., Garza, V., Carter, P., Alexoff, D., Logan, J., et al., 2003. Evaluation of a new norepinephrine transporter PET ligand in baboons, both in brain and peripheral organs. Synapse 50, 345–352.

Ding, Y.-S., Lin, K.S., Logan, J., Benveniste, H., Carter, P., 2005. Comparative evaluation of positron emission tomography radiotracers for imaging the norepinephrine transporter: (S, S) and (R, R) enantiomers of reboxetine analogs ([11C]methylreboxetine, 3-Cl-[11C]methylreboxetine and [18F]fluororeboxetine), (R)-[11C]nisoxetine, [11C] oxaprotiline and [11C]lortalamine. J. Neurochem. 94, 337–351.

Ding, Y.-S., Lin, K.S., Logan, J., 2006. PET imaging of norepinephrine transporters [review]. Curr. Pharm. Des. 12, 3831–3845.

Dopheide, J.A., Pliszka, S.R., 2009. Attention-deficit-hyperactivity disorder: an update. Pharmacotherapy 29, 656–679.

Eagle, D.M., Bari, A., Robbins, T.W., 2008. The neuropsychopharmacology of action inhibition: cross-species translation of the stop-signal and go/no-go tasks. Psychopharmacology (Berl) 199, 439–456.
Faraone, S.V., Biederman, J., Spencer, T., Michelson, D., Adler, L., Reimherr, F., Glatt, S.J., 2005. Efficacy of atomoxetine in adult attention-deficit/hyperactivity disorder: a drug–placebo response curve analysis. Behav. Brain Funct. 1, 16.
Gallezot, J.D., Weinzimmer, D., Nabulsi, N., Lin, S.F., Fowles, K., Sandiego, C., et al., 2011. Evaluation of [^{11}C]MRB for assessment of occupancy of norepinephrine transporters: studies with atomoxetine in non-human primates. NeuroImage 56, 268–279.
Hannestad, J., Gallezot, J.-D., Planeta-Wilson, B., Lin, S.-F., Williams, W., van Dyck, C.H., Malison, R.T., Ding, Y.-S., 2010. Clinically relevant doses of methylphenidate significantly occupy norepinephrine transporters in humans in vivo. Biol. Psychiatry 6, 854–860.
Hinz, R., Selvaraj, S., Murthy, N.V., Bhagwagar, Z., Taylor, M., Cowen, P.J., Grasby, P.M., 2008. Effects of citalopram infusion on the serotonin transporter binding of [^{11}C] DASB in healthy controls. J. Cereb. Blood Flow Metab. 28, 1478–1490.
Horrigan, J.P., Barnhill, L.J., 1995. Guanfacine for treatment of attention-deficit-hyperactivity disorder in boys. J. Child Adolesc. Psychopharmacol. 5, 215–223.
Houle, S., Ginovart, N., Hussey, D., Meyer, J.H., Wilson, A.A., 2000. Imaging the serotonin transporter with positron emission tomography: initial human studies with [11C] DAPP and [11C]DASB. Eur. J. Nucl. Med. 27, 1719–1722.
Huang, Y., Hwang, D.R., Narendran, R., Sudo, Y., Chatterjee, R., Bae, S.A., et al., 2002. Comparative evaluation in nonhuman primates of five PET radiotracers for imaging the serotonin transporters: [^{11}C]McN 5652, [^{11}C]ADAM, [^{11}C]DASB, [^{11}C]DAPA, and [^{11}C] AFM. J. Cereb. Blood Flow Metab. 22, 1377–1398.
Hunt, R.D., Arnsten, A.F., Asbell, M.D., 1995. An open trial of guanfacine in the treatment of attention deficit hyperactivity disorder. J. Am. Acad. Child Adolesc. Psychiatry 34, 50–54.
Ichise, M., Toyama, H., Innis, R.B., Carson, R.E., 2002. Strategies to improve neuroreceptor parameter estimation by linear regression analysis. J. Cereb. Blood Flow Metab. 22, 1271–1281.
Johnson, C.A., Thada, S., Rodriguez, M., Zhao, Y., Iano-Fletcher, A.R., Liow, J., Barker, W.C., Martino, R.L., Carson, R.E., 2004. Software architecture of the MOLAR-HRRT reconstruction engine. IEEE Nuclear Science Symposium Conference Record 6, 3956–3960.
Kish, S.J., Furukawa, Y., Chang, L.J., Tong, J., Ginovart, N., Wilson, A., et al., 2005. Regional distribution of serotonin transporter protein in postmortem human brain: is the cerebellum a SERT-free brain region? Nucl. Med. Biol. 32, 123–128.
Lassen, N.A., Bartenstein, P.A., Lammertsma, A.A., Prevett, M.C., Turton, D.R., Luthra, S.K., Osman, S., et al., 1995. Benzodiazepine receptor quantification in vivo in humans using [^{11}C]flumazenil and PET: application of the steady-state principle. J. Cereb. Blood Flow Metab. 15, 152–165.
Lijffijt, M., Kenemans, J.L., Verbaten, M.N., van Engeland, H., 2005. A metaanalytic review of stopping performance in attention-deficit/hyperactivity disorder: deficient inhibitory motor control? J. Abnorm. Psychol. 114, 216–222.
Ma, C.-L., Qi, X.-L., Peng, J.-Y., Li, B.-M., 2003. Selective deficit in no-go performance induced by blockade of prefrontal cortical alpha2-adrenoceptors in monkeys. Neuroreport 14, 1013–1016.
Michelson, D., Faries, D., Wernicke, J., Kelsey, D., Kendrick, K., Sallee, F.R., Spencer, T., 2001. Atomoxetine ADHD Study Group. Atomoxetine in the treatment of children and adolescents with attention-deficit/hyperactivity disorder: a randomized, placebo-controlled, dose–response study. Pediatrics 108, E83.
O'Sullivan, J.B., Ryan, K.M., Curtin, N.M., Harkin, A., Connor, T.J., 2009. Noradrenaline reuptake inhibitors limit neuroinflammation in rat cortex following a systemic inflammatory challenge: implications for depression and neurodegeneration. Int. J. Neuropsychopharmacol. 12, 687–699.
Parsey, R.V., Kent, J.M., Oquendo, M.A., Richards, M.C., Pratap, M., Cooper, T.B., Arango, V., et al., 2006. Acute occupancy of brain serotonin transporter by sertraline as measured by [^{11}C]DASB and positron emission tomography. Biol. Psychiatry 59, 821–828.
Ring, B.J., Gillespie, J.S., Eckstein, J.A., Wrighton, S.A., 2002. Identification of the human cytochromes P450 responsible for atomoxetine metabolism. Drug Metab. Dispos. 30, 319–323.
Robbins, T.W., Arnsten, A.F., 2009. The neuropsychopharmacology of fronto-executive function: monoaminergic modulation. Annu. Rev. Neurosci. 32, 267–287.
Sauer, J.-M., Ponsler, G.D., Mattiuz, E.L., Long, A.J., Witcher, J.W., Thomasson, H.R., Desante, K.A., 2003. Disposition and metabolic fate of atomoxetine hydrochloride: the role of CYP2D6 in human disposition and metabolism. Drug Metab. Dispos. 31, 98–107.
Scahill, L., Chappell, P.B., Kim, Y.S., et al., 2001. Guanfacine in the treatment of children with tic disorders and ADHD: a placebo-controlled study. Am. J. Psychiatry 158, 1067–1074.
Swanson, C.J., Perry, K.W., Koch-Krueger, S., Katner, J., Svensson, K.A., Bymaster, F.P., 2006. Effect of the attention deficit/hyperactivity disorder drug atomoxetine on extracellular concentrations of norepinephrine and dopamine in several brain regions of the rat. Neuropharmacology 50, 755–760.
Szabo, Z., McCann, U.D., Wilson, A.A., Scheffel, U., Owonikoko, T., Mathews, W.B., et al., 2002. Comparison of (+)-(11)C-McN5652 and (11)C-DASB as serotonin transporter radioligands under various experimental conditions. J. Nucl. Med. 43, 678–692.
Tatsumi, M., Groshan, K., Blakely, R.D., Richelson, E., 1997. Pharmacological profile of antidepressants and related compounds at human monoamine transporters. Eur. J. Pharmacol. 340, 249–258.
Volkow, N.D., Wang, G.W., Fowler, J.S., Logan, J., Gerasimov, M., Maynard, L., Ding, Y.-S., Gatley, S.J., Gifford, A., Franceschi, D., 2001. Therapeutic doses of oral methylphenidate significantly increase extracellular dopamine in the human brain. J. Neurosci. 21, RC121.